Electronic Supplementary Information

Experimental section

Materials: Nickel foam (NF) was provided by Hangxu Filters Flag Store, Hengshui, Hebei. 4,4'-Biphenyl dicarboxylic acid ($C_{14}H_{10}O_4$) was purchased from Shanghai Haohong Scientific Co., Ltd. N,N-dimethylformamide (DMF) and $NiCl_2 \cdot 6H_2O$ were purchased from Aladdin Ltd. in Shanghai. Hydrochloric acid (HCl) and C_2H_5OH were purchased from Chengdu Kelon Chemical Reagent Factory. RuO_2 was purchased from Shanghai Macklin Biochemical Co., Ltd. Nafion (5 wt%) solution was purchased from Sigma-Aldrich Chemical Reagent Co., Ltd. All chemical regents were used as received without further purification. The water used throughout all experiments was purified through a Millipore system.

Preparation of the Ni-MOF/NF: The in situ growth of Ni-MOF nanosheet array on NF was carried out via a one-step solvothermal reaction. A piece of NF was first treated with 1 M HCl, ethanol and deionized water by ultrasonic cleaning sequentially before use. 0.4 mmol $NiCl_2 \cdot 6H_2O$ (0.0951 g) and 0.4 mmol $C_{14}H_{10}O_4$ (0.0969 g) were dissolved in 25 mL DMF to form a solution, 2.5 mL ethanol and 2.5 mL deionized water were added slowly to the solution under constant stirring. Then the solution was transferred to a 40 mL Teflon-lined stainless-steel autoclave in which a piece of treated NF (2.5 × 4 cm) was immersed into the solution. The autoclave was sealed and maintained at 125 ℃ for 8 h in an electric oven to obtain Ni-MOF/NF. After the autoclave cooled down naturally, the Ni-MOF/NF was taken out and washed with water and ethanol for several times, followed by drying 12 h at 60 ℃.

Preparation of the RuO_2/NF: 20 mg commercial RuO_2 and 40 μL 5 wt% Nafion solution were dispersed in 960 μL ethanol/water (v/v = 3:1) followed by 30 min sonication to form a homogeneous ink. Then 20 μL ink was loaded onto a NF (0.5 × 0.5 cm) and dried under ambient condition (RuO_2 loading: 1.6 mg cm^{-2}). The Ni-MOF powder/NF electrode was also prepared according to above method.

Characterizations: XRD pattern was obtained from a Shimazu XRD-6100 diffractometer with Cu Kα radiation (40 kV, 30 mA) of wavelength 0.154 nm (Japan).

XPS measurements were performed on an ESCALABMK II X-ray photoelectron spectrometer using Mg as the exciting source. SEM measurements were carried out on a XL30 ESEM FEG scanning electron microscope at an accelerating voltage of 20 kV.

Electrochemical measurements: Electrochemical measurements were performed with a CHI 660E potentiostat (CH Instruments, China) in a standard three-electrode setup with the prepared samples as the working electrode, a graphite rod as the counter electrode, the Hg/HgO electrode as the reference electrode. The OER activity was evaluated using linear sweep voltammetry (LSV) with a sweep rate of 5 mV s^{-1}. Electrochemical impedance spectroscopy (EIS) was measured at a frequency between 0.1 Hz and 10^6 Hz. The tests were performed in 1 M KOH Solution. All the potentials were displayed versus reversible hydrogen electrode (RHE) by the formula: E (RHE) = E (Hg/HgO) + 0.098 + 0.059 × pH.

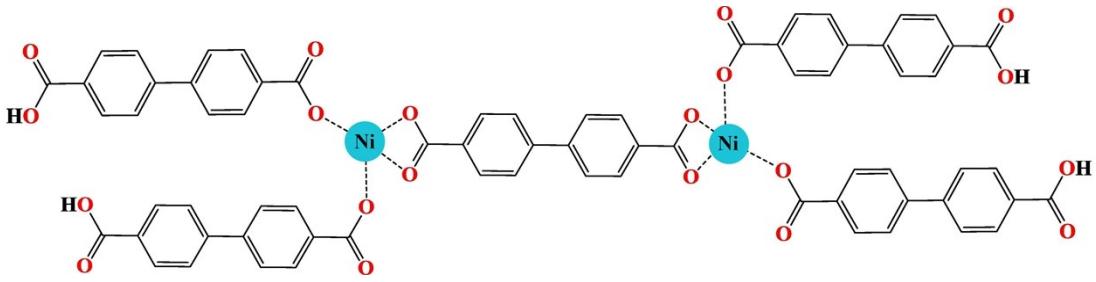

Fig. S1. Atomic structural diagram of Ni-MOF.

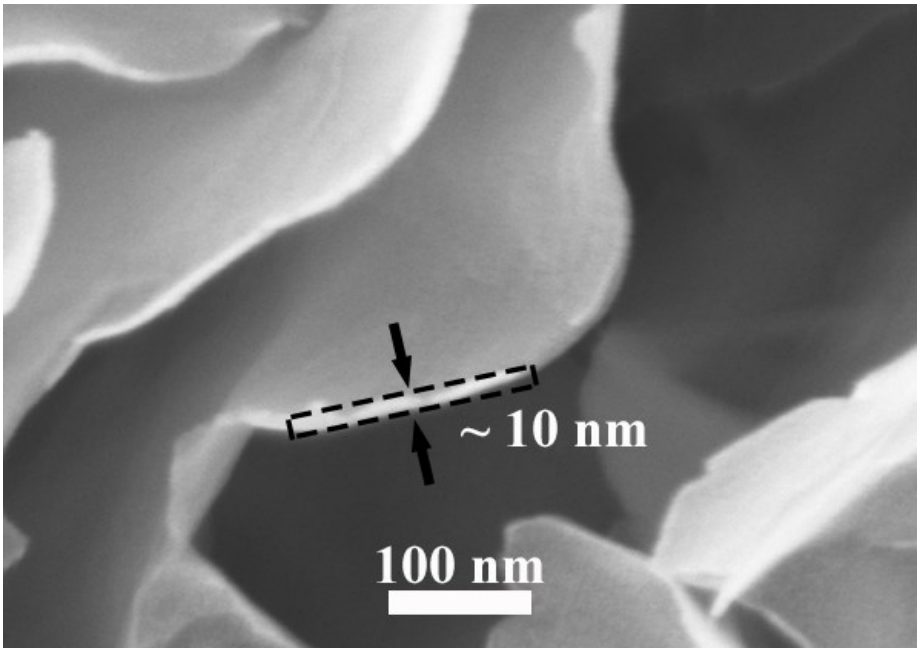

Fig. S2. SEM image of Ni-MOF nanosheet.

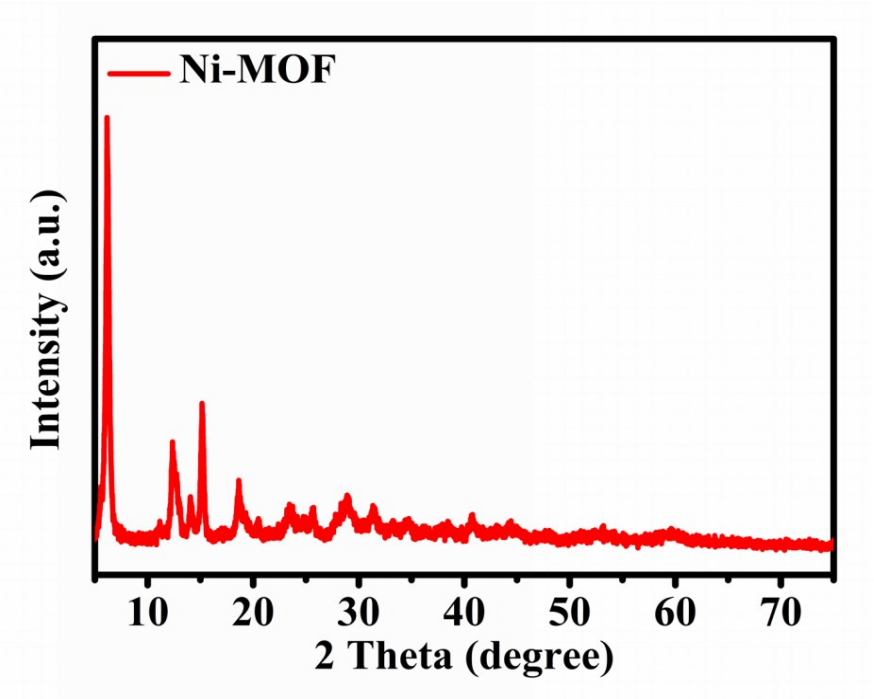

Fig. S3. XRD pattern for Ni-MOF scratched down from NF.

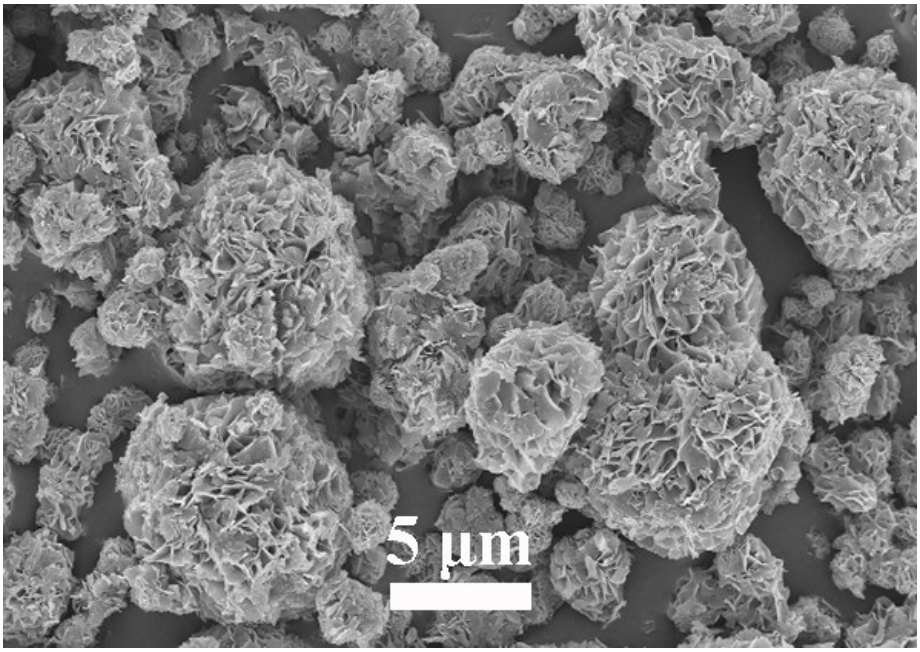

Fig. S4. SEM image of Ni-MOF powder.

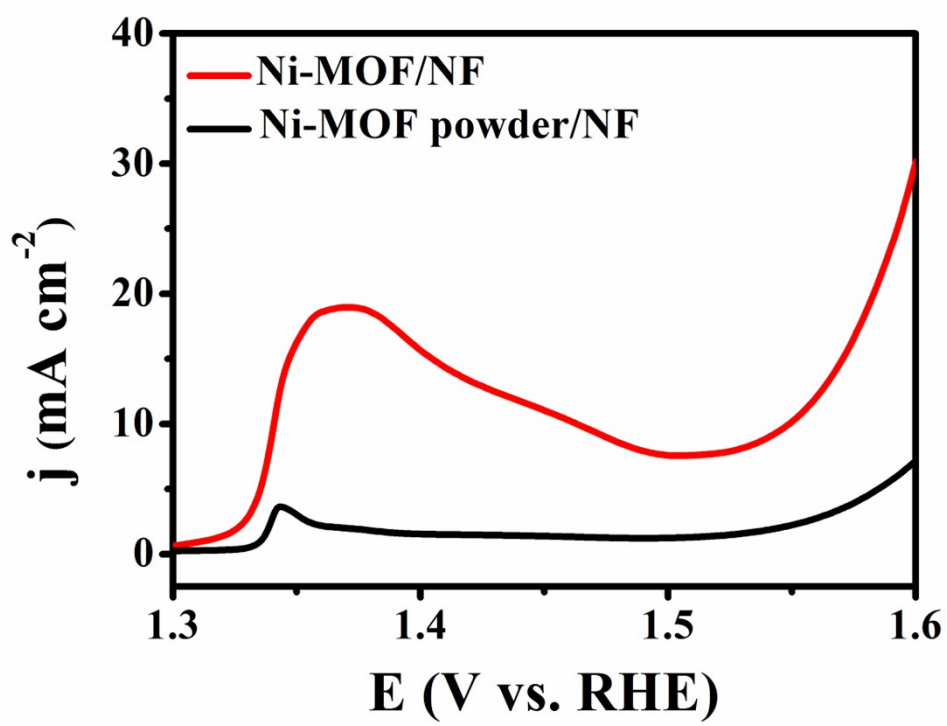

Fig. S5. A local view of the LSV curves for Ni-MOF/NF and Ni-MOF powder/NF.

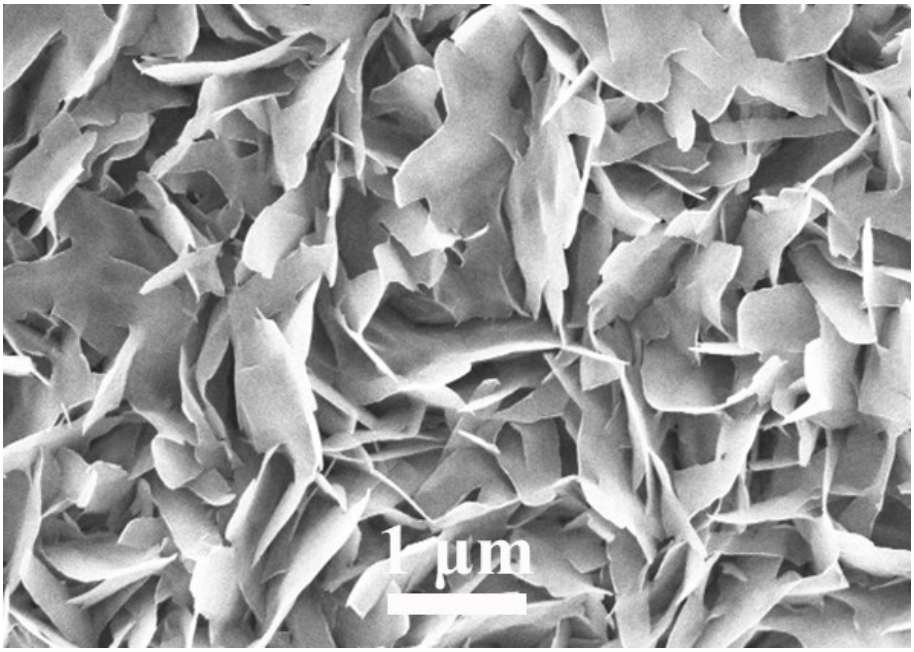

Fig. S6. SEM image of Ni-MOF/NF after the oxidation of Ni^{2+} to Ni^{3+} before OER.

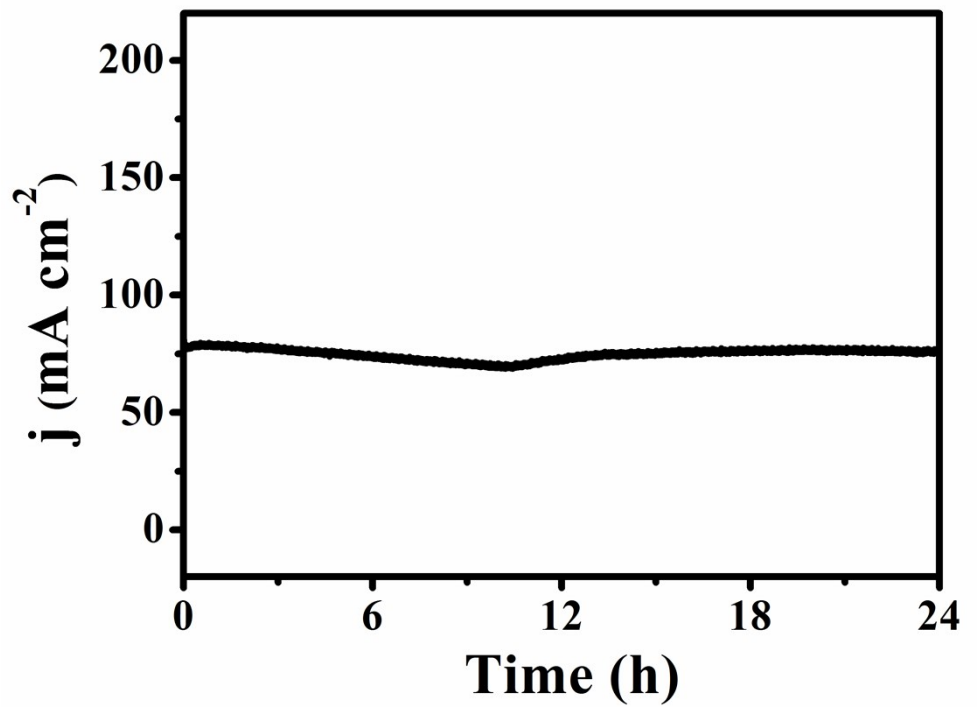

Fig. S7. Time-dependent current density curve for Ni-MOF/NF.

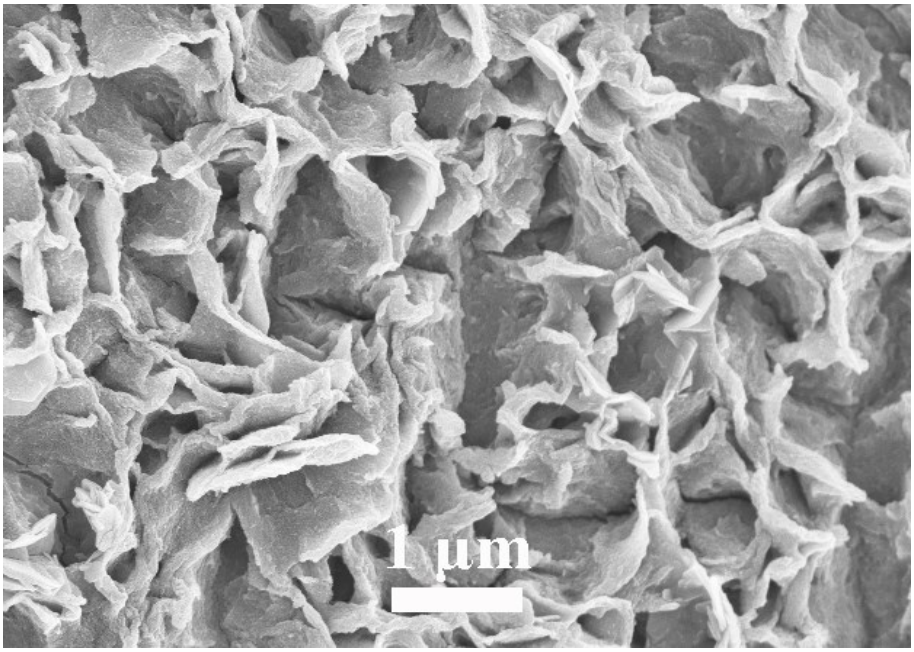

Fig. S8. SEM image of Ni-MOF/NF after OER electrolysis.

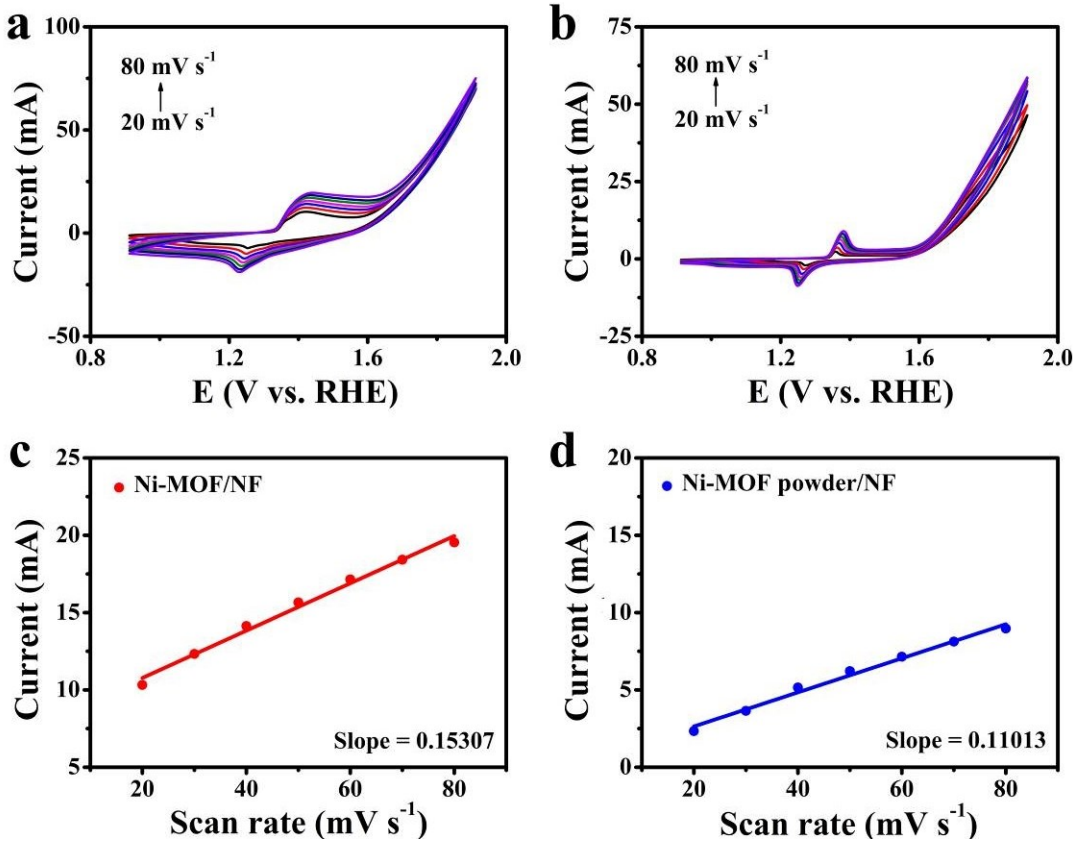

Fig. S9. CVs of (a) Ni-MOF/NF and (b) Ni-MOF powder/NF under different scan rates increasing from 20 to 80 mV s^{-1} in 1.0 M KOH. Linear relationship of the oxidation peak currents vs. scan rates for (c) Ni-MOF/NF and (d) Ni-MOF powder/NF.

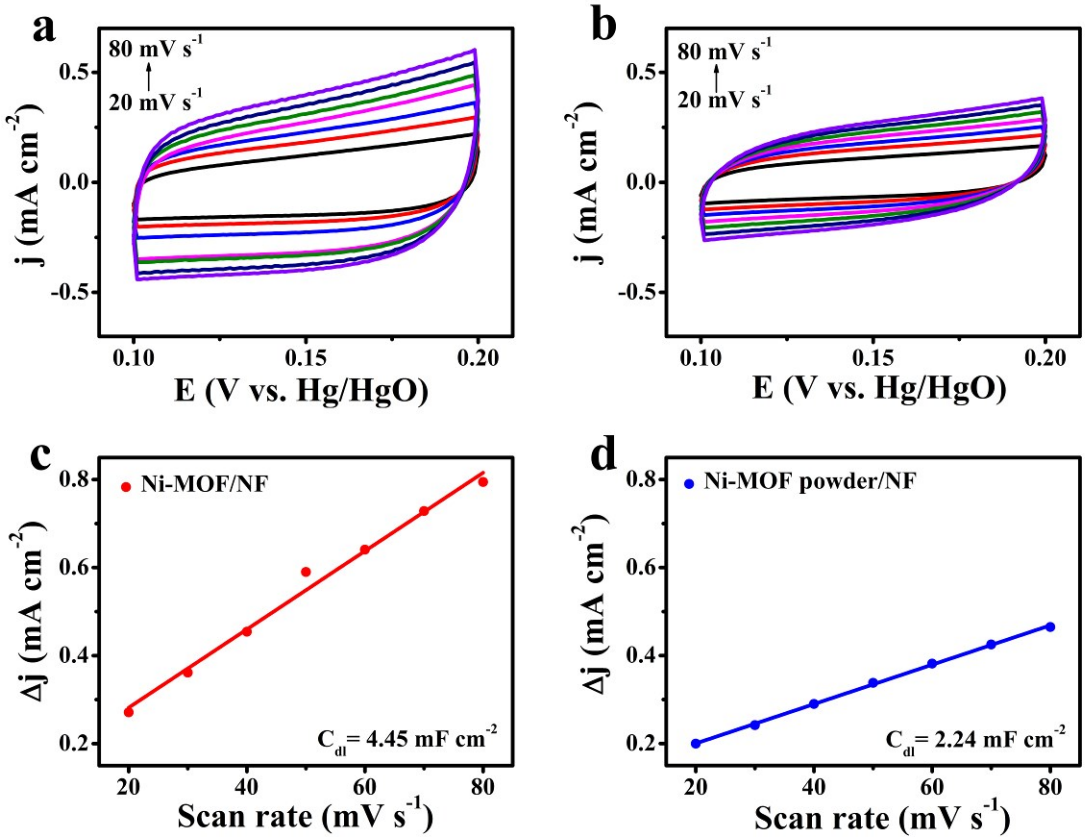

Fig. S10. (a) Ni-MOF/NF and (b) Ni-MOF powder/NF in the non-faradaic capacitance current range at scan rates increasing from 20 to 80 mV s^{-1}. (c) and (d) the capacitive currents at 0.15 V vs. Hg/HgO as a function of scan rate for Ni-MOF/NF and Ni-MOF powder/NF.

Table S1. Comparison of OER performance for Ni-MOF/NF with other Ni-based electrocatalysts in alkaline media.

Catalyst	j (mA cm^{-2})	η (mV)	Electrolyte	Ref.
Ni-MOF/NF	20/100	350/450	1.0 M KOH	This work
Ni_3N/NF	100	470	1.0 M KOH	1
Ni/CTF	10	374	1.0 M KOH	2
ALD NiS_x	10	372	1.0 M KOH	3
β-$Ni(OH)_2$	10	444	1.0 M KOH	4
NiOOH	10	525	1.0 M KOH	5
NiOOH nanosheets	10	~370	1.0 M KOH	6
NiO/NF	10	390	1.0 M KOH	7
Ni-MOF/NF	10	362	1.0 M KOH	8
Co_xNi_{7-x}	10	370	1.0 M KOH	9
NiCo LDH	10	367	1.0 M KOH	10
CoNi SUNOE	10	450	1.0 M KOH	11
$NiCo_2O_4$ nanoneedles	10	565	1.0 M KOH	12
Fe-Ni oxide	10	>375	1.0 M KOH	13
Fe_3Pt/Ni_3FeN	10	370	1.0 M KOH	14

References

1 M. Shalom, D. Ressnig, X. Yang, G. Clavel, T. P. Fellinger and M. Antonietti, Nickel nitride as an efficient electrocatalyst for water splitting, *J. Mater. Chem. A*, 2015, **3**, 8171–8177.

2 S. Ozturk, Y. Xiao, D. Dietrich, B. Giesen, J. Barthel, J. Ying, X. Yang and C. Janiak, Nickel nanoparticles supported on a covalent triazine framework as electrocatalyst for oxygen evolution reaction and oxygen reduction reactions, *Beilstein J. Nanotechnol.*, 2020, **11**, 770–781.

3 H. Li, Y. Shao, Y. Su, Y. Gao and X. Wang, Vapor-phase atomic layer deposition of nickel sulfide and its application for efficient oxygen-evolution electrocatalysis, *Chem. Mater.*, 2016, **28**, 1155–1164.

4 M. Gao, W. Sheng, Z. Zhuang, Q. Fang, S. Gu, J. Jiang and Y. Yan, Efficient water oxidation using nanostructured alpha-nickel-hydroxide as an electrocatalyst, *J. Am. Chem. Soc.*, 2014, **136**, 7077–7084.

5 S. Klaus, Y. Cai, M. W. Louie, L. Trotochaud and A. T. Bell, Effects of Fe electrolyte impurities on $Ni(OH)_2$/NiOOH structure and oxygen evolution activity, *J. Phys. Chem. C*, 2015, **119**, 7243–7254.

6 Y. Jin, S. Huang, X. Yue, C. Shu and P. Shen, Highly stable and efficient non-precious metal electrocatalysts of Mo-doped NiOOH nanosheets for oxygen evolution reaction, *Int. J. Hydrogen Energy*, 2018, **43**, 12140–12145.

7 G. Han, Y. Liu, W. Hu, B. Dong, X. Li, X. Shang, Y. Chai, Y. Liu and C. Liu, Three dimensional nickel oxides/nickel structure by in situ electro-oxidation of nickel foam as robust electrocatalyst for oxygen evolution reaction, *Appl. Surf. Sci.*, 2015, **359**, 172–176.

8 X. Wang, B. Li, Y. Wu, A. Tsamis, H. Yu, S. Liu, J. Zhao, Y. Li and D. Li, Investigation on the component evolution of a tetranuclear nickel-cluster-based metal-organic framework in an electrochemical oxidation reaction, *Inorg. Chem.*, 2020, **59**, 4764–4771.

9 D. Cai, A. Han, P. Yang, Y. Wu, P. Du, M. Kurmoo and M. Zeng, Heptanuclear Co, Ni and mixed Co-Ni clusters as high-performance water oxidation electrocatalysts, *Electrochim. Acta*, 2017, **249**, 343–352.

10 H. Liang, F. Meng, M. Caban-Acevedo, L. Li, A. Forticaux, L. Xiu, Z. Wang and S. Jin, Hydrothermal continuous flow synthesis and exfoliation of NiCo layered double hydroxide nanosheets for enhanced oxygen evolution catalysis, *Nano Lett.*, 2015, **15**, 1421–1427.

11 B. Ni and X. Wang, Edge overgrowth of spiral bimetallic hydroxides ultrathin-nanosheets for water oxidation, *Chem. Sci.*, 2015, **6**, 3572–3576.

12 H. Shi and G. Zhao, Water oxidation on spinel $NiCo_2O_4$ nanoneedles anode: microstructures, specific surface character, and the enhanced electrocatalytic performance, *J. Phys. Chem. C*, 2014, **118**, 25939–25946.

13 J. Landon, E. Demeter, N. İnoğlu, C. Keturakis, I. E. Wachs, R. Vasić, A. I. Frenkel and J. R. Kitchin, Spectroscopic characterization of mixed Fe–Ni oxide electrocatalysts for the oxygen evolution reaction in alkaline electrolytes, *ACS Catal.*, 2012, **2**, 1793–1801.

14 Z. Cui, G. Fu, Y. Li and J. B. Goodenough, Ni_3FeN-supported Fe_3Pt intermetallic nanoalloy as a high-performance bifunctional catalyst for metal-air batteries, *Angew. Chem., Int. Ed.*, 2017, **56**, 9901–9905.